

# Pragmatic hydraulic theory predicts stomatal responses to climatic water deficits

John S. Sperry<sup>1</sup>, Yujie Wang<sup>1</sup>, Brett T. Wolfe<sup>2</sup>, D. Scott Mackay<sup>3</sup>, William R. L. Anderegg<sup>1</sup>, Nate G. McDowell<sup>4</sup> and William T. Pockman<sup>5</sup>

<sup>1</sup>Department of Biology, University of Utah, Salt Lake City, UT 84112, USA; <sup>2</sup>Smithsonian Tropical Research Institute, PO Box 0843-03092, Balboa, Panama; <sup>3</sup>Department of Geography, State University of New York, Buffalo, NY 14260, USA; <sup>4</sup>Earth and Environmental Sciences Division, Los Alamos National Lab, Los Alamos, NM 87545, USA; <sup>5</sup>Biology Department, University of New Mexico, Albuquerque, NM 87131, USA

## Summary

Author for correspondence:

John S. Sperry

Tel: +1 801 585 0379

Email: j.sperry@utah.edu

Received: 8 February 2016

Accepted: 13 May 2016

*New Phytologist* (2016) **212**: 577–589

doi: 10.1111/nph.14059

**Key words:** climate change drought, hydraulic limitation, modeling climate change impacts, plant drought responses, plant water transport, stomatal regulation, xylem cavitation, xylem transport.

- Ecosystem models have difficulty predicting plant drought responses, partially from uncertainty in the stomatal response to water deficits in soil and atmosphere. We evaluate a 'supply–demand' theory for water-limited stomatal behavior that avoids the typical scaffold of empirical response functions. The premise is that canopy water demand is regulated in proportion to threat to supply posed by xylem cavitation and soil drying.
- The theory was implemented in a trait-based soil–plant–atmosphere model. The model predicted canopy transpiration ( $E$ ), canopy diffusive conductance ( $G$ ), and canopy xylem pressure ( $P_{\text{canopy}}$ ) from soil water potential ( $P_{\text{soil}}$ ) and vapor pressure deficit ( $D$ ).
- Modeled responses to  $D$  and  $P_{\text{soil}}$  were consistent with empirical response functions, but controlling parameters were hydraulic traits rather than coefficients. Maximum hydraulic and diffusive conductances and vulnerability to loss in hydraulic conductance dictated stomatal sensitivity and hence the iso- to anisohydric spectrum of regulation. The model matched wide fluctuations in  $G$  and  $P_{\text{canopy}}$  across nine data sets from seasonally dry tropical forest and piñon–juniper woodland with < 26% mean error.
- Promising initial performance suggests the theory could be useful in improving ecosystem models. Better understanding of the variation in hydraulic properties along the root–stem–leaf continuum will simplify parameterization.

## Introduction

Stomatal pores control rates of terrestrial photosynthesis and transpiration, particularly under water-limited conditions. Partial or complete stomatal closure reduces plant water stress, but at the cost of reduced productivity, elevated heat, light, and pest stress, leaf shedding, and mortality. Climate change is predicted to cause more frequent and intense droughts in many regions (Dai, 2011), yet current ecosystem models poorly capture observed drought responses (Allen *et al.*, 2010; Powell *et al.*, 2013). It is important to have an accurate and efficient way of predicting stomatal responses to water deficits if we are to improve our poor ability to model responses to drought. The stimulus–response pathways that underlie stomatal adjustments are not fully understood at the mechanistic and molecular levels (Buckley & Mott, 2013). But we can still predict stomatal behavior from its emergent properties. In this paper, we evaluate a theory of water-limited stomatal regulation that is based on the balance of water supply and demand (Sperry & Love, 2015).

As soon as John Milburn began listening to acoustic emissions from xylem cavitation, the implications for stomatal regulation

were recognized (Milburn, 1973, 1979). It has become accepted that stomatal closure in response to water deficits in soil and atmosphere is associated with protecting the xylem from excessive cavitation (Field & Holbrook, 1989; Sparks & Black, 1999; Tombesi *et al.*, 2015). Supply–demand theory formalizes this concept (Sperry & Love, 2015).

On the supply side, the transpiration stream is delivered to the leaves by the cohesion–tension mechanism (Pickard, 1981; Brown, 2013). This physical process is directly coupled to soil and atmospheric water deficits (Fig. 1a). Soil dryness dictates the upstream water pressure for the transpiration stream. Atmospheric dryness determines the potential rate of flow and the downstream pressure. More negative pressures increase flow resistance by causing cavitation in xylem conduits, and draining of soil pores in the rhizosphere (Fig. 1b). The dangerous feedback between falling pressure and rising flow resistance has been modeled for many years (Tyree & Sperry, 1988; Jones & Sutherland, 1991; Sperry *et al.*, 1998) and is referred to as a vascular 'supply function' (Fig. 1c; Sperry & Love, 2015).

The supply function is the steady-state relationship between rising transpiration rate ( $E$ ) and consequently falling canopy

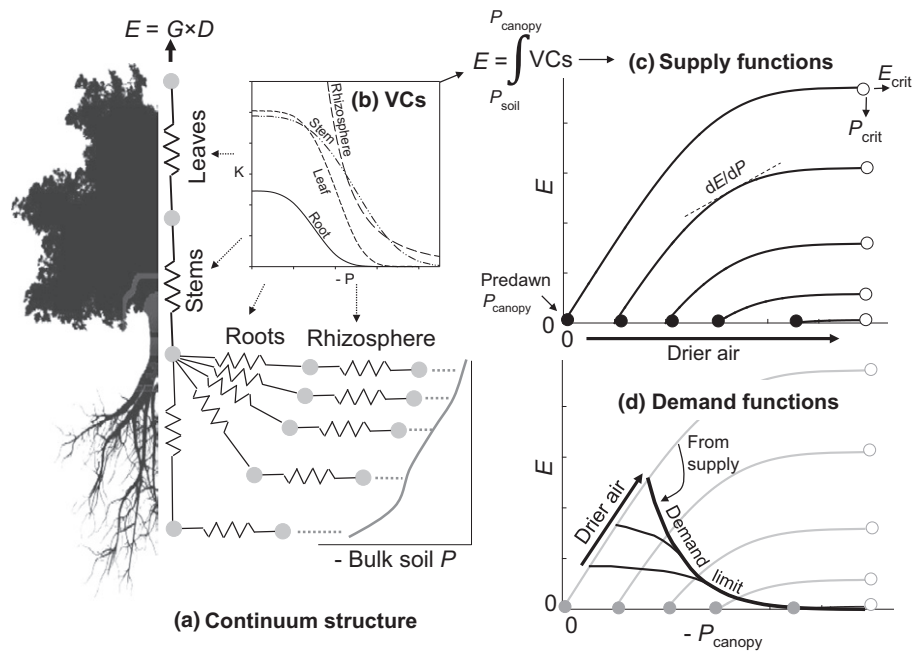


**Fig. 1** The supply–demand model. (a) A conductance network links layers of bulk soil ( $P_{\text{soil}}$  = soil water potential) via rhizosphere and root paths to the stem and leaves. (b) Each network component has a vulnerability curve (VC) describing its drop in hydraulic conductance ( $k$ ) with more negative pressure ( $P$ ). (c) Integrating network vulnerability curves across the pressure drop from  $P_{\text{soil}}$  to  $P_{\text{canopy}}$  yields a vascular supply function: steady-state transpiration rate ( $E$ ) vs  $P_{\text{canopy}}$ . These functions rise from a predawn  $P_{\text{canopy}}$  at  $E = 0$  to  $E_{\text{crit}}$  (at corresponding  $P_{\text{crit}}$ ). The  $dE/dP$  derivative (dashed tangent) reflects the canopy hydraulic conductance, which goes to zero at the  $E_{\text{crit}}$  hydraulic limit. As soil dries out, the predawn intercept (closed circles) becomes more negative and  $E_{\text{crit}}$  (open circles) drops. (d) A demand function derived from the supply function determines the stomatal regulation of  $E$  in response to drier air (which pushes the plant up its supply function) and dry soil (which shrinks the supply function). The demand function yields a physiological ‘demand limit’ that saturates  $E$  below  $E_{\text{crit}}$ .

xylem pressure ( $P_{\text{canopy}}$ ) for constant soil water potential (Fig. 1c, curves rising from predawn  $P_{\text{canopy}}$  symbol). The supply function can be calculated by integrating ‘vulnerability curves’ that describe the loss of hydraulic conductance with negative pressure (Fig. 1b, ‘VCs’; Sperry & Love, 2015). The derivative of the supply function,  $dE/dP_{\text{canopy}}$  (Fig. 1c, dashed  $dE/dP$  tangent), is proportional to the hydraulic conductance at the canopy end of the flow path. The  $dE/dP_{\text{canopy}}$  falls to zero beyond a maximum  $E$  (Fig. 1c,  $E_{\text{crit}}$  symbol) as cavitation increases and blocks flow. Drier soil truncates the supply function and diminishes  $E_{\text{crit}}$  ultimately to zero (Fig. 1c, ‘drier soil’ arrow). The supply function extends to lower pressures when the xylem is more resistant to cavitation and when there is greater root surface area to minimize resistance to flow across the rhizosphere (Sperry *et al.*, 1998, 2002a).

On the transpiration demand side, the theory proposes a ‘stomatal demand function’ (the ‘loss function’ of Sperry & Love, 2015) that locates the plant on its shifting supply function (Fig. 1d). The demand function represents the emergent coordination between leaf water supply and atmospheric water demand as limited by stomatal regulation. Stomatal regulation of  $E$  should not allow  $E_{\text{crit}}$  to be exceeded because this would prematurely desiccate the canopy and leave usable water in the soil. Even approaching  $E_{\text{crit}}$  is risky, because the accelerating decline in  $dE/dP_{\text{canopy}}$  increases the cavitation consequences of minor  $E$  fluctuations. Nevertheless, the plant should exploit its ability to

extract soil water and sustain  $E$  as far into a soil drought as  $E_{\text{crit}}$  permits. The demand function explained in Sperry & Love (2015) (their fig. 2) has stomatal closure reducing  $P_{\text{canopy}}$  in proportion to the loss of canopy hydraulic conductance (quantified by the decline in  $dE/dP_{\text{canopy}}$ ) that would occur without closure. The more environmental conditions threaten the pipeline, the greater the protective response. The result is a physiological limit to the stomatal demand that keeps  $E$  safely below the  $E_{\text{crit}}$  limit regardless of the dryness of soil or air (Fig. 1d, ‘demand limit’ curve). The system only fails hydraulically if the predawn  $P_{\text{canopy}}$  drops enough to drive  $E_{\text{crit}}$  to zero.

The supply–demand theory occupies a unique place among attempts to model stomatal behavior. It is not a mechanistic model of stimulus–response control at the molecular or physiological scale (Tardieu & Davies, 1993; Li *et al.*, 2006; Buckley & Mott, 2013; Franks, 2013). It is not an empirical model with coefficients divorced from physiological process (Jarvis, 1976; Ball *et al.*, 1987; Stewart, 1988; Lloyd, 1991; Leuning, 1995). Although it is based on an adaptive, emergent property of stomata (the balance of water demand with limited supply), it is not an optimization model like that of Cowan (Cowan, 1977; Medlyn *et al.*, 2011), which is based on an unknown variable ( $\lambda$ , the marginal carbon cost of water loss). Models that assume a near-isohydric  $P_{\text{canopy}}$  (Williams *et al.*, 1996; Sperry *et al.*, 2002a; Pieruschka *et al.*, 2010) capture the priority of avoiding damage-inducing negative pressure, but fail to account for anisohydric

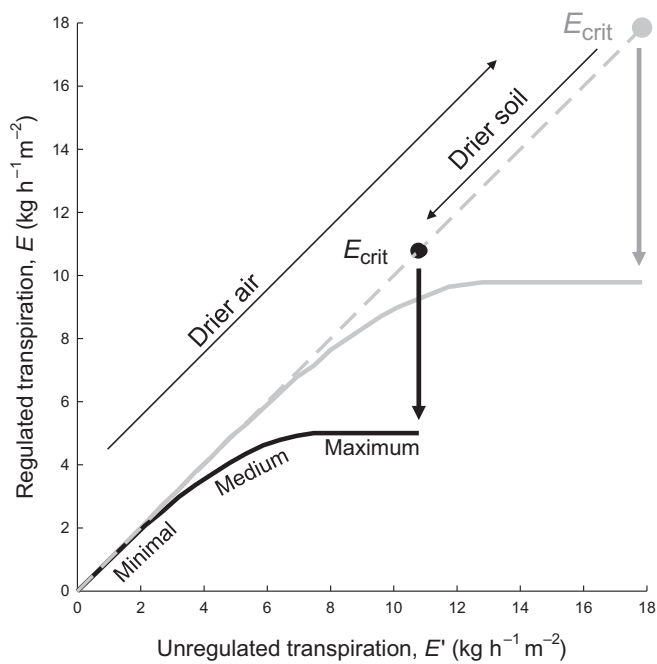


**Fig. 2** Theoretical modes of transpiration ( $E$ ) regulation (solid curves) relative to no regulation (gray dashed diagonal). When air is humid, unregulated transpiration ( $E'$ , representing maximum stomatal opening) is low, there is little threat of cavitation, and hence there is little stomatal closure, resulting in minimal regulation of  $E$  ( $E \approx E'$ , near the dashed no-regulation diagonal). As air becomes drier,  $E'$  increases along with the threat of cavitation, triggering greater stomatal closure that deflects the solid curve from the dashed diagonal. *Medium* regulation slows the rise in  $E$  relative to  $E'$ , followed in the driest air by maximum regulation, which keeps  $E$  constant and below the hydraulic limit at  $E_{crit}$  (vertical arrows from  $E_{crit}$  symbols). Drier soil reduces  $E_{crit}$  (compare gray (wet) and dry (black)  $E_{crit}$  symbols), intensifies the threat of cavitation, and intensifies stomatal closure in response to drier air (gray vs black solid curves).

behavior where  $P_{canopy}$  drops during water deficits. The TREES model is the closest to supply–demand theory because it uses the cavitation-based supply function to set a hydraulic limit to  $E$  (Mackay *et al.*, 2015). However, it still requires an empirical model of the stomatal response to vapor pressure deficit ( $D$ ; Oren *et al.*, 1999).

How good is supply–demand theory? We implement the theory in a model for predicting stomatal regulation of  $E$  and  $P_{canopy}$ , and evaluate its behavior and realism. The model is kept simple while still incorporating heterogeneous soil and xylem properties (Fig. 1a). We compare model output with observed trends and empirical functions of stomatal responses to  $D$  and soil drought. Shortcuts are examined that minimize parameterization and simplify application. We test the model’s ability to explain observed variation in canopy diffusive conductance ( $G$ , for water vapor) and  $P_{canopy}$  in nine data sets drawn from tropical forests with pronounced dry seasons (Wolfe *et al.*, 2016) and from semiarid piñon-juniper woodlands (McDowell *et al.*, 2013).

## Description

The model is written in Visual Basic for Applications in Excel (download from <http://biologylabs.utah.edu/sperry/methods.html>)

and in C (GCC 5.3, GNU Project). It predicts steady-state solutions at a given  $D$  and bulk-soil water potential ( $P_{soil}$ ) profile. Table 1 summarizes the parameters.

## Representation of the soil–plant continuum

The continuum divides leaf, stem, root, and rhizosphere components in series (Fig. 1a). The rhizosphere is the soil around each root through which water moves down a pressure gradient from a constant-pressure water source in ‘bulk’ soil. The root and rhizosphere can be divided into up to  $N$  parallel components draining  $N$  horizontal soil layers (Fig. 1a).

**Table 1** Model input/output, default settings, and low vs high test range

Variable	Default setting (low, high)
<i>Inputs for supply function</i>	
$P_{soil}$ , bulk soil matric potential in $N$ layers per time step	0 MPa (0, –8 MPa)
Continuum $k_{max}$ (no cavitation, saturated soil)	10 kg h <sup>–1</sup> MPa <sup>–1</sup> m <sup>–2</sup> (3, 42)
Average % resistance in rhizosphere (from $P = 0$ to $P_{crit}$ )	5% (5, 50)
Weibull function $b$ and $c$ for root, stem, leaf (Eqn 1) <sup>1</sup>	$b = 2, c = 3$ , not segmented ( $b = 1, 4, c = 3$ sigmoid; segmented) ( $b = 1.27, c = 1$ exponential)
Van Genuchten function $\alpha$ and ‘ $n$ ’ (Eqn 2)	$\alpha = 602$ MPa <sup>–1</sup> , $n = 1.48$ (sandy clay loam)
Reversibility of cavitation (yes/no)	no (no, yes)
Prior drought $P_{soil}$ (irreversible cavitation only)	0 MPa (–2)
<i>Inputs for demand function</i>	
$D$ , leaf-to-air vapor pressure deficit per time step	1 kPa (0.1, 4.9)
$G_{max}$ , maximum canopy diffusive conductance to H <sub>2</sub> O	2130 kg h <sup>–1</sup> m <sup>–2</sup> (512, 3200)
<i>Inputs for continuum structure</i>	
% resistance of root, stem, leaf at continuum $k_{max}$	50, 25, 25% (not tested)
Root depth coefficient, $\beta$	0.92 (not tested)
Root radial spread per maximum depth	1 (not tested)
Number of root and soil layers, $N$	1 (1, 5)
<i>Output (per time step)</i>	
Predawn and current $P_{canopy}$ (xylem pressure)	–MPa
$E$ , canopy transpiration rate	kg h <sup>–1</sup> m <sup>–2</sup>
$G$ , canopy diffusive conductance	kg h <sup>–1</sup> m <sup>–2</sup>
$E_{crit}$ , physical maximum transpiration rate	kg h <sup>–1</sup> m <sup>–2</sup>
$P_{crit}$ , physical minimum canopy xylem pressure	–MPa
Current stem and root crown $P$	–MPa
Hydraulic conductance of rhizosphere, root, stem, leaf	kg h <sup>–1</sup> MPa <sup>–1</sup> m <sup>–2</sup>
Root water uptake from each of $N$ layers	kg h <sup>–1</sup> m <sup>–2</sup>

<sup>1</sup>Not segmented, identical root–stem–leaf curves; segmented, roots and/or leaves more vulnerable. Sigmoid curves retained the same  $c$  parameter (Eqn 1); exponential curves had  $b$  and  $c$  parameters creating a nonthreshold drop from  $k_{max}$ .

Each continuum component has a vulnerability curve that starts at a maximum hydraulic conductance ( $k_{\max}$ , flow rate per pressure drop) and declines as water pressure ( $P$ ) becomes more negative (Fig. 1b). Xylem components (leaf, stem, root) were assigned a two-parameter Weibull function:

$$k = k_{\max} e^{[-((P/b)^c)]}, \quad \text{Eqn 1}$$

where  $k$  is the hydraulic conductance of the component and  $P$  is the negative sap pressure in the xylem of the component (absolute value for convenience). Parameter  $b$  ( $P$  at  $k/k_{\max} = 0.37$ ) shifts the curve along the pressure axis, parameter  $c$  controls shape ('exponential' shape with no threshold has  $c \leq 1$ , sigmoidal threshold has  $c > 1$ ). In 'nonsegmented' mode, xylem components have the same curve vs 'segmented' mode where curves differ. The rhizosphere was assigned a van Genuchten function (van Genuchten, 1980):

$$k = k_{\max} v^{(n-1)/2n} \left[ (1 - v)^{(n-1)/n} - 1 \right]^2 \quad \text{Eqn 2a}$$

$$v = [(\alpha P_{\text{soil}})^n + 1]^{-1}, \quad \text{Eqn 2b}$$

where  $n$  and  $\alpha$  are texture-specific parameters (Leij *et al.*, 1996), and  $P_{\text{soil}}$  is the absolute value of the soil water potential (assuming negligible osmotic potential). Eqn 2 is termed a 'rhizosphere vulnerability curve' by analogy with the xylem. Neither Eqn 1 nor 2 reaches mathematical zero, but we assumed  $k < 0.05\%$  of continuum  $k_{\max}$  was physiological zero. Sap viscosity was assumed constant.

### The vascular supply function

The steady-state flow rate through each component,  $E_i$ , is related to the flow-induced pressure drop across that component (downstream pressure ( $P_{\text{down}}$ ) – upstream pressure ( $P_{\text{up}}$ )) by the integral transform of the component's vulnerability curve ( $k(P)_i$  from Eqns 1 and 2):

$$E_i = P_{\text{up}} \int_{P_{\text{down}}}^{P_{\text{up}}} k(P)_i dP. \quad \text{Eqn 3}$$

The integral transform assumes infinite discretization of the flow path, equivalent to infinitely short conduits. This is a reasonable approximation for many plants (Comstock & Sperry, 2000).

Eqn 3 is used to compute the supply function for the continuum (Fig. 1c). When there is one soil layer, the rhizosphere, root, stem, and leaf are in series. The  $E_i$  is identical for each component and equal to canopy  $E$ . The  $P_{\text{soil}}$  is known. Thus, from any  $E = E_i$ , the sequential pressure drops across each component are obtained from its individual integral transform (Eqn 3; excluding the gravitational drop). By solving  $P_{\text{canopy}}$  in this way as  $E$  is increased from zero, the  $E(P_{\text{canopy}})$  supply function is calculated.

When the root and rhizosphere components are partitioned into  $N$  parallel paths draining  $N$  soil layers of known  $P_{\text{soil}}$ , there are  $N+1$  unknown pressures: the  $N$  root surface pressures

(rhizosphere  $P_{\text{down}} = \text{root } P_{\text{up}}$ ) and the root crown pressure at the downstream junction for all root components (root  $P_{\text{down}}$ ). The  $N+1$  unknown pressures were solved from the following  $N+1$  equations for steady-state flow:

$$E_{i(\text{rhizosphere})} - E_{i(\text{root})} = 0 \quad \text{Eqn 4a}$$

$$\sum E_{i(\text{root})} - E = 0, \quad \text{Eqn 4b}$$

where  $E_i$  values were obtained from Eqn 3, and  $E$  was specified. Eqns 4(a) ( $N$  equations for  $N$  layers) and 4(b) ( $E_i$  sum over  $N$  layers) were solved using multidimensional Newton Raphson (Press *et al.*, 1989). Stem and leaf pressures were then obtained from Eqn 3 and the supply function generated by incrementing  $E$  from zero.

### The stomatal demand function

The demand function calculates  $E$  and  $G$  (canopy diffusive conductance to water vapor) from the atmospheric  $D$  (mole fraction),  $G_{\max}$  (representing maximally open stomata and prevailing boundary layer conditions), and the supply function. The demand function derived in Sperry & Love (2015) (illustrated in their Fig. 2) has five steps. (1) The unregulated  $E' = DG_{\max}$  is located on the supply function. (2) The loss of canopy hydraulic conductance that would be caused by  $E'$  was determined from the decline in the derivative of the supply function from its maximum at  $P_{\text{canopy}} = P_{\text{soil}}$  ( $dE/dP_{\max}$ ) to its value at  $E'$  ( $dE'/dP_{\text{canopy}}$ ). The  $(dE'/dP_{\text{canopy}})/(dE/dP_{\max})$  fraction falls from 1 at no conductance loss to 0 for total loss at  $E_{\text{crit}}$ ; its value represents the loss of canopy transport capacity caused by doing nothing and leaving the stomata open. (3) The unregulated soil to canopy pressure drop,  $\Delta P'$ , is reduced by the  $(dE'/dP_{\text{canopy}})/(dE/dP_{\max})$  fraction to yield the regulated pressure drop:

$$\Delta P = \Delta P' [(dE'/dP_{\text{canopy}})/(dE/dP_{\max})]. \quad \text{Eqn 5}$$

Mathematically,  $\Delta P$  rises to a maximum before decreasing back to zero as  $E'$  increases to  $E_{\text{crit}}$ . This decline in  $\Delta P$  is unrealistic (Saliendra *et al.*, 1995), so it is assumed that  $\Delta P$  saturates at its maximum as  $E'$  increases. Eqn 5 expresses the outcome that xylem pressure is regulated in proportion to the damage caused by taking no action. (4) The regulated  $E$  corresponding to  $\Delta P$  is determined from the supply function. (5) The  $G$  is solved from  $E/D$  to determine how much it is reduced below  $G_{\max}$ . The model does not partition  $G$  into stomatal vs boundary layer components, but  $G$  is controlled by stomatal regulation. Cuticular water loss is assumed to be zero.

### Reversible vs irreversible cavitation

The model runs in reversible and irreversible cavitation modes. In reversible mode, xylem hydraulic conductances track the original vulnerability curves ( $k(P) = \text{Eqn 1}$ ) regardless of  $P$  fluctuation. In irreversible mode, the drop in xylem conductance is permanent, and the  $k(P)$  vulnerability curves change from the original.

For  $P=0$  to  $P_{\min}$  (most negative  $P$  already experienced by the conductance element),  $k=k(P_{\min})$ . For  $P$  more negative than  $P_{\min}$ , the  $k(P)=\text{Eqn 1}$ . The supply function changes accordingly. Importantly, the demand function still calculates  $\Delta P$  from the original uncavitated supply function: this assumes that the protective regulation of xylem pressure is immutably set by the inherent vulnerability of the continuum. The regulated  $E$ , however, is calculated from the current supply function as impacted by cavitation. This produces the realistic result that past cavitation does not influence  $\Delta P$ , but does reduce  $E$  (e.g., Hacke *et al.*, 2000; Anderegg *et al.*, 2013, 2014). When running in irreversible cavitation mode, the model can be initialized to prior exposure to a minimum  $P_{\text{soil}}$  (Table 1). Rhizosphere vulnerability curves were fully reversible in either cavitation mode.

### Maximum hydraulic conductances ( $k_{\max}$ )

The maximum hydraulic conductance of the continuum in the absence of any cavitation (continuum  $k_{\max}$ ) is an input parameter, as is its division into root, stem, and leaf  $k_{\max}$  components as required for Eqn 1. Rhizosphere  $k_{\max}$  (i.e. saturated soil) was large enough to be a negligible component of continuum  $k_{\max}$ . Hydraulic conductances were usually expressed per trunk basal area. Hence the transpiration rate and canopy diffusive conductance to water vapor ( $G=E/D$ ) were also expressed per trunk basal area.

We solved for the rhizosphere  $k_{\max}$  from an inputted 'average % rhizosphere resistance.' The % of continuum resistance in the rhizosphere was calculated from the in-series vulnerability curves of rhizosphere, root, stem, and leaf at the same  $P$  (Eqns 1, 2). The % rhizosphere resistance was averaged over 0.1 MPa increments from  $P=0$  to  $P_{\text{crit}}$ . The rhizosphere % was negligible at  $P=0$  but can become significant with more negative  $P$  because of the steep drop in the rhizosphere vulnerability curve (Eqn 2). The lower the % average rhizosphere resistance, the greater the area of absorbing roots per trunk basal area, and the thinner the rhizosphere. We specified rhizosphere resistance (via rhizosphere  $k_{\max}$ ; Eqn 2) rather than calculating it from rhizosphere geometry and root area (as in Sperry *et al.*, 1998).

Root and rhizosphere components could be partitioned into  $N$  paths draining horizontal soil layers. Layer depths were set so each layer included equal root biomass based on the function (Jackson *et al.*, 1996):

$$B = 1 - \beta^d, \quad \text{Eqn 6}$$

where  $B$  is the fraction of biomass above depth  $d$  in cm, and  $0 < \beta < 1$ . Maximum root depth was set at  $B=0.995$  (99.5% root biomass). The rhizosphere  $k_{\max}$  for the whole root system was partitioned equally among the  $N$  layers. Total root system  $k_{\max}$  was divided among layers in proportion to the inverse of the transport distance to each layer. Transport distance was depth to the center of layer biomass plus the radial spread of roots within each layer. The radial spread for the top layer was calculated by multiplying maximum root depth by an inputted aspect ratio of

maximum radial spread divided by maximum root depth. The rooted soil volume in the top layer was calculated as a cylinder from spread and layer thickness. By assuming this volume was constant for each layer, the radial root spread in deeper soil layers was calculated.

### Comparison of measured vs modeled $P_{\text{canopy}}$ and $G$

We tested the model against nine published data sets (Table 2; methods detailed in McDowell *et al.*, 2013; Wolfe *et al.*, 2016) consisting of vulnerability curves, soil type, and a time course of predawn  $P_{\text{canopy}}$  and midday  $P_{\text{canopy}}$ ,  $D$ , and  $G$  measured on individual trees and on sunny days (summary data in Supporting Information Table S1). All data sets included major drought events. The 'tropical tree' data sets (Wolfe *et al.*, 2016) consisted of seven, 2 yr time-courses, split between three species in a tropical dry forest (pronounced dry season) and four species in a tropical transitional forest (moderate dry season). One species was common between sites (Table 2). Each time course was assembled by averaging four to 10 trees per species/site. Species/site-specific vulnerability curves were only available for stems ( $P_{50}$  values (pressure at 50% loss of hydraulic conductance), cited in Table 2; curves in Fig. S1), so the model was not segmented. The piñon (*Pinus edulis*) and juniper (*Juniperus monosperma*) data sets (McDowell *et al.*, 2013) consisted of 4 yr time-courses (April–October growing season) for six trees per species. Fluxes and conductances were on a sapwood area basis. Vulnerability curves were available for stems (both species) and roots (*P. edulis*).

The model was set to  $N=1$  soil layer with  $P_{\text{soil}}=$ measured predawn  $P_{\text{canopy}}$ , and it was run for each time series of predawn pressure and midday  $D$  to predict midday  $P_{\text{canopy}}$  and  $G$ . Predicting from predawn xylem pressure eliminated having to specify root system depth and aspect ratio, soil layers, and  $P_{\text{soil}}$  profile.

The model was fitted to each data set via adjustment of three unknown inputs: the % rhizosphere resistance, continuum  $k_{\max}$ , and  $G_{\max}$ . Although the data sets included  $k$  and  $G$  (Table S1), they did not include conditions maximizing them (high light, very low  $D$ , and prolonged wet periods). No prior drought input was necessary because test runs confirmed its influence was largely compensated for by the tuning of  $k_{\max}$ ,  $G_{\max}$ , and % rhizosphere (Methods S1). To equalize weighting across  $G$  and  $P_{\text{canopy}}$ , each value was 'studentized' by subtracting the respective measurement mean and dividing by the standard deviation. The absolute error averaged across studentized  $G$  and  $P_{\text{canopy}}$  was minimized by adjusting  $G_{\max}$ ,  $k_{\max}$ , and % rhizosphere with the downhill simplex algorithm, making every effort to ensure global minimums were found (Nelder & Mead, 1965; Methods S1). Although  $G$  and  $P_{\text{canopy}}$  were fitted simultaneously, we report individual  $G$  and  $P_{\text{canopy}}$  mean absolute errors and  $r^2$  values. Best fits were found for irreversible vs reversible cavitation settings. The piñon and juniper data sets were fitted at the individual tree level and subdivided into separate years to allow for off-season adjustments in the three fitting parameters (McDowell *et al.*, 2013). Best-fit results for each tree were pooled to obtain the species fit.

**Table 2** Model fit statistics for the nine data sets as plotted in Fig. 9. The model was run in irreversible cavitation mode

Data set	$P_{\text{canopy error}}^1$		$G_{\text{error}}^1$		$r^2$ (for $P$ ) <sup>2</sup>	$r^2$ (for $G$ ) <sup>2</sup>	Sample size	$G_{\text{max}}, G_{\text{average}}^3$	$SD^{+4}$	$k_{\text{max}}, k_{\text{average}}^3$	$SD^{+4}$	% rhiz <sup>5</sup>	P50 <sup>6</sup>
	Mean	%	Mean	%									
<i>Annona hayesii</i> , transitional dry <sup>7</sup>	0.21	11.4	132.5	38.5	0.94	0.73	$P = 16, G = 17$	1135, 344	2.1	17.5, 5.1	5.7	82	4.59
<i>Astronium graveolens</i> , transitional dry <sup>7</sup>	0.39	23.3	76.9	31.8	0.60	0.56	$P = 16, G = 17$	312, 242	0.42	4.1, 4.8	-0.1	53	4.38
<i>Bursera simaruba</i> , dry <sup>7</sup>	0.13	18.4	59.8	74.4	0.35	0.30	$P = 15, G = 17$	380, 80	2.3	99.6, 20.8	2.8	77	1.31
<i>Cavanillesia platanifolia</i> , transitional dry <sup>7</sup>	0.08	14.1	57.6	32.7	0.43	0.93	$P = 12, G = 15$	754, 176	2.7	39.2, 10.6	2.6	65	3.10
<i>Cojoba rufescens</i> , transitional dry <sup>7</sup>	0.27	13.5	53.1	13.3	0.73	0.89	$P = 16, G = 17$	787, 400	1.6	6.4, 5.4	0.2	56	4.63
<i>C. rufescens</i> , dry <sup>7</sup>	0.34	14.6	181	33.9	0.78	0.69	$P = 16, G = 17$	3030, 534	6.0	33.8, 15.9	1.0	72	2.80
<i>Genipa americana</i> , dry <sup>7</sup>	0.25	12.4	96.1	33.8	0.90	0.75	$P = 14, G = 14$	4251, 284	14.5	100, 9.5	10.7	86	2.04
<i>Juniperus monosperma</i> <sup>8</sup>	0.50	12.5	17.7	31.3	0.87	0.77	$P = 165, G = 165$	188, 57	2.3	7.93, 2.23	2.8	67	7.90
<i>Pinus edulis</i> <sup>8</sup>	0.48	18.6	27.7	36.0	0.30	0.70	$P = 134, G = 134$	540, 77	5.3	15.4, 4.0	2.3	43	2.75

<sup>1</sup> $P_{\text{canopy error}}$  (MPa),  $G_{\text{error}}$  ( $G, \text{kg h}^{-1} \text{m}^{-2}$ ) are mean absolute errors (and % of observed mean).

<sup>2</sup> $r^2$  values for canopy xylem pressure and canopy diffusive conductance outputs.

<sup>3</sup> $G_{\text{max}}, G_{\text{average}}, k_{\text{max}}, k_{\text{average}}$  ( $\text{kg h}^{-1} \text{m}^{-2}$ ), best-fit values for maximum  $G$  and soil-canopy hydraulic conductance,  $k$ , and the mean measured value of  $G$  and  $k$ .

<sup>4</sup> $SD^{+4}$ , number of standard deviations above mean for  $G_{\text{max}}$  and  $k_{\text{max}}$ .

<sup>5</sup>% rhiz, best-fit value for the average % rhizosphere hydraulic resistance.

<sup>6</sup>P50, xylem pressure at 50% loss of hydraulic conductance from measured stem vulnerability curves (–MPa).

<sup>7</sup>'Dry' and 'transitional' refer to the forest type (Wolfe *et al.*, 2016).

<sup>8</sup>McDowell *et al.* (2013).

## Results

### Three modes of transpiration ( $E$ ) regulation

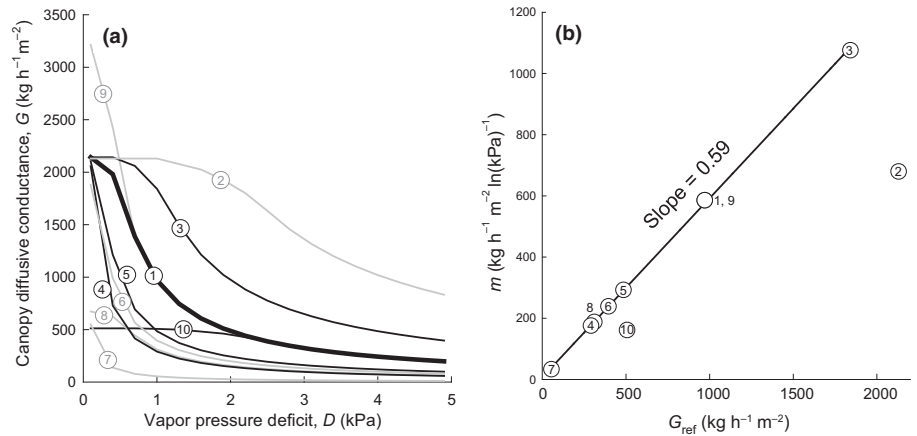
The behavior of  $E$  in response to  $D$  and  $P_{\text{soil}}$  was determined for default settings (Table 1). The demand function produced three modes of  $E$  regulation (Fig. 2). When  $D$  was low, there was little threat from canopy cavitation ( $(dE/dP_{\text{canopy}})/(dE/dP_{\text{max}}) \approx 1$ ), resulting in minimal regulation where regulated  $E \approx$  unregulated  $E'$  (Fig. 2 'minimal' portion of curve). As  $D$  rose and the threat of canopy cavitation increased ( $[(dE/dP_{\text{canopy}})]/[dE/dP_{\text{max}}] < 1$ ), medium regulation slowed the rise in  $E$  relative to  $E'$  (Fig. 2 'medium'). At highest  $D$ , the threat of cavitation was maximized ( $(dE/dP_{\text{canopy}})/(dE/dP_{\text{max}})$  approached 0), and maximum regulation capped  $E$  at a physiological limit well within the physical limit of  $E_{\text{crit}}$  (Fig. 2 'maximum'). Soil drying suppressed  $E_{\text{crit}}$ , intensified regulation, and caused reduction in the physiological  $E$  limit (Fig. 2 compare grey vs black curves). The regulation of  $E$  (Fig. 2) yielded the stomatal control of canopy diffusive conductance ( $G = E/D$ ). At minimal regulation,  $G \approx G_{\text{max}}$ , and at maximum regulation  $G$  fell in inverse proportion to  $D$ .

### Stomatal response to $D$

The stomatal response to  $D$  was obtained by incrementing  $D$  while holding other inputs constant. The default response (Fig. 3a, curve 1; settings in Table 1) showed the typical reduction in  $G$  from  $G_{\text{max}}$  in response to increasing  $D$ . However, the  $D$  threshold causing  $G < G_{\text{max}}$  depended on model inputs as documented in a full sensitivity analysis (Figs S2, S3). Key trends are evident from changing inputs one at a time from the default to high vs low ends of the test range indicated in Table 1. Inputs that increased the  $D$  threshold for stomatal closure were: increased continuum  $k_{\text{max}}$  (Fig. 3a, curve 2), a more resistant sigmoid vulnerability curve (curve 3;  $b$  from 2 to 4; Table 1), and lower  $G_{\text{max}}$  (curve 10). Inputs that accelerated stomatal closure were: lower  $k_{\text{max}}$  (curve 4), a weaker sigmoid vulnerability curve (curve 5;  $b$  from 2 to 1), an exponential vulnerability curve (curve 6,  $b = 1.27$ ,  $c = 1$ ), drier soil (curve 7;  $P_{\text{soil}} = -2$  MPa), exposure to prior drought without xylem refilling (curve 8;  $P_{\text{soil}} = 0$  after exposure to  $P_{\text{soil}} = -2$  MPa), and increasing  $G_{\text{max}}$  (curve 9). Increasing the average % rhizosphere resistance (from 5% to 50%; Table 1) had no effect because rhizosphere resistance at default  $P_{\text{soil}} = 0$  is always 0%.

The  $G$  by  $D$  response curves in Fig. 3(a) compared well with empirical functions used to model the  $D$  response. In these comparisons, the  $D$  range was restricted to 1–4 kPa (incremented by 0.3 kPa) to exclude extremes not well represented by observation. Within this range,  $G$  exactly followed the equation,  $G = g_1/D$  ( $g_1 =$  fitted coefficient; Lloyd, 1991), as expected during maximum regulation when  $G \ll G_{\text{max}}$  (curves 1 and 3–9;  $r^2 = 1.0$ ). This inverse model broke down for minimal-to-medium regulation when  $G$  was near  $G_{\text{max}}$  (curves 2 and 10), even when adding the additional fitting

**Fig. 3** Theoretical response of diffusive conductance ( $G$ ) via stomatal closure to vapor pressure deficit ( $D$ ). (a)  $G$  vs  $D$  curves for default vs test settings in Table 1. Curve 1, default; 2, high  $k_{\max}$ ; 3, high sigmoid cavitation resistance; 4, low  $k_{\max}$ ; 5, low sigmoid cavitation resistance; 6, exponential cavitation resistance; 7, dry soil; 8, wet soil, post-drought; 9, high  $G_{\max}$ ; 10, low  $G_{\max}$ . (b) Curves in 'a' fit with empirical function:  $G = G_{\text{ref}} - m \ln D$ . The greater the value of  $G_{\text{ref}}$  ( $G$  at  $D = 1$  kPa), the greater is the rate of closure,  $m$ , with a slope of 0.59. Only when there is minimal regulation, as in curves 2 and 10, do points fall below this slope. This mimics observations (Oren *et al.*, 1999).



coefficient  $g_o$ :  $G = g_o + g_1/D$  ( $r^2 = 0.79$ ). Maximum regulation was also closely approximated ( $r^2 = 0.98-0.99$ ) by the inverse square root function:  $G = g_o + g_1/D^{1/2}$  (Lloyd, 1991), and the hyperbolic function:  $G = g_o + g_1/(1 + D)$  (Leuning, 1995). These functions gave improved fits for minimal-to-medium regulation ( $r^2 = 0.86-0.88$ ). The final empirical model tested was the equation  $G = G_{\text{ref}} - m \ln(D)$ , where  $G_{\text{ref}}$  is  $G$  at  $D = 1$  kPa (Oren *et al.*, 1999). This was the least tight of the functions for maximum regulation ( $r^2 = 0.93$ ), but comparable to the best for minimal-to-medium regulation ( $r^2 = 0.86$ ). Greater  $G_{\text{ref}}$  has been observed to covary tightly with increasing  $m$  with a highly conserved slope of 0.56–0.6. This slope is predicted for maximum regulation, where  $P_{\text{canopy}}$  is being homeostatically regulated (Oren *et al.*, 1999). Shallower slopes coincide with less strict regulation that allows  $E$  to increase (and  $P_{\text{canopy}}$  to become more negative). Consistent with observation, the slope of  $G_{\text{ref}}$  vs  $m$  was 0.59 for maximum regulation (Fig. 3b, curves 1, 3–9), and the response fell below the 0.59 slope for minimal-to-medium regulation (Fig. 3b, curves 2, 10).

**Stomatal response to soil moisture deficit ( $P_{\text{soil}}$ )**

The stomatal response to  $P_{\text{soil}}$  was obtained by holding  $D$  constant and decrementing  $P_{\text{soil}}$  from 0 to  $-8$  MPa. Closure in drier soil occurred with varying sensitivity relative to the default response (Fig. 4, curve 1). Trends from the sensitivity analysis (Fig. S4) are illustrated by altering settings one at a time exactly as for the  $D$  response (numbered curves in Figs 3 and 4 have identical settings). Inputs that increased  $G$  relative to the default curve were: greater continuum  $k_{\max}$  (Fig. 4 curve 2), a more resistant sigmoid vulnerability curve (curve 3), and a lower  $D$  (curve 12; 0.5 kPa vs default of 1.0 kPa). Increasing  $G_{\max}$  had no effect because  $G$  was already below  $G_{\max}$  in the default. Inputs that decreased  $G$  were: reduced  $k_{\max}$  (curve 4), a weaker sigmoid vulnerability curve (curve 5), the exponential vulnerability curve (curve 6), previous exposure to drought (curve 8), greater  $D$  (curve 13; 4 kPa), and lower  $G_{\max}$  (curve 10). In drying soil, an increase in the average rhizosphere resistance also caused more closure (curve 11).

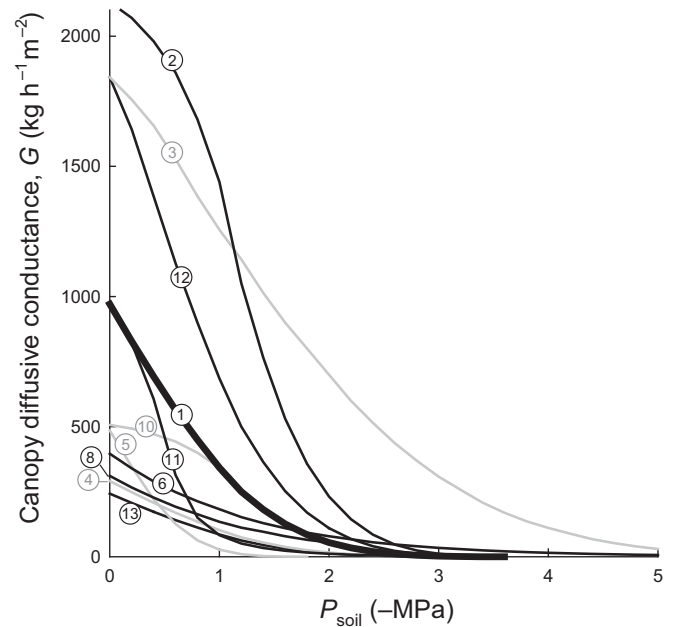


**Fig. 4** Theoretical response of diffusive conductance ( $G$ ) via stomatal closure to soil water potential ( $P_{\text{soil}}$ ). Curves 1–10 correspond to Fig. 3 (curve 1, default; 2, high  $k_{\max}$ ; 3, high sigmoid cavitation resistance; 4, low  $k_{\max}$ ; 5, low sigmoid cavitation resistance; 6, exponential cavitation resistance; 7, dry soil; 8, wet soil, post-drought; 9, high  $G_{\max}$ ; 10, low  $G_{\max}$ ). Curve 11, greater % rhizosphere resistance; curve 12, reduced  $D$  (from 1 to 0.5 kPa); curve 13, increased  $D$  (from 1 to 4 kPa).

**Regulation of xylem pressure ( $P_{\text{canopy}}$ ) in response to drought**

Plotting midday  $P_{\text{canopy}}$  vs predawn  $P_{\text{canopy}}$  ( $= P_{\text{soil}}$ ) from the  $P_{\text{soil}}$  responses of Fig. 4 revealed diverse stomatal regulation of xylem pressure in response to drought (Fig. 5). The  $G_{\max}$ ,  $k_{\max}$ , and  $D$  settings had no effect on  $\Delta P$  once  $E$  was capped by maximum regulation. Hence, low  $G_{\max}$  (or, alternatively, high  $k_{\max}$ ) and low  $D$  only limited  $E$  and  $\Delta P$  in wetter soil (Fig. 5, curves 12 and 10).

Vulnerability curves largely dictated  $P_{\text{canopy}}$  regulation. A higher % rhizosphere resistance (50%) sharply limited  $\Delta P$  in medium dry soil (Fig. 5, curve 11). A more vulnerable sigmoidal xylem curve reduced the  $\Delta P$  and drove it to zero at less negative  $P_{\text{soil}}$  (curve 5). Conversely, a more resistant sigmoidal curve was

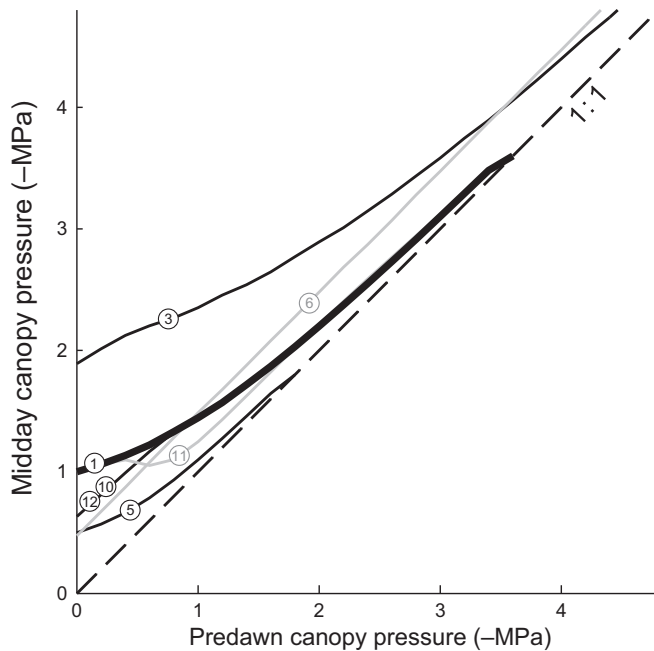


**Fig. 5** Theoretical response of midday canopy xylem pressure ( $P_{\text{canopy}}$ ) to predawn canopy pressure. Curves are as follows: 1, default; 2, high  $k_{\text{max}}$ ; 3, high sigmoid cavitation resistance; 4, low  $k_{\text{max}}$ ; 5, low sigmoid cavitation resistance; 6, exponential cavitation resistance; 7, dry soil; 8, wet soil, post-drought; 9, high  $G_{\text{max}}$ ; 10, low  $G_{\text{max}}$ ; 11, greater % rhizosphere resistance; 12, reduced  $D$  (from 1 to 0.5 kPa); 13, increased  $D$  (from 1 to 4 kPa).

associated with a greater  $\Delta P$ , which declined to zero at more negative  $P_{\text{soil}}$  (curve 3). The exponential vulnerability curve produced a near-constant  $\Delta P$  (curve 6), because its flat tail produced relatively little cavitation and a near-constant  $dE/dP$  derivative.

The usually curved theoretical midday vs predawn  $P_{\text{canopy}}$  relationship was approximated by a linear regression to compare simulated slope and intercept with observations (Martínez-Vilalta *et al.*, 2014; Fig. 6). Regressions excluded extreme tails of droughted plants with > 75% loss of plant hydraulic conductance (assumed rare in observations). Default inputs were used except for the Weibull vulnerability curve. Simulated predawn vs midday slopes increased from 0.2 (more isohydric) to 1.2 (extreme anisohydric) as the Weibull shape parameter  $c$  decreased from extreme sigmoid ( $c=20$ ) to extreme exponential ( $c=0.7$ ; dashed horizontal curves). This encompassed nearly the full range of observed slopes (Fig. 6, gray symbols). Simulated intercepts ( $\Delta P$  at  $P_{\text{soil}}=0$ ) increased from  $c. 0.5$  MPa to > 2.5 MPa as the ' $b$ ' parameter increased from 1 (vulnerable) to 9 (resistant; vertical solid curves). Intercepts were capped at 2.7 MPa when default  $G_{\text{max}}$  increasingly limited wet soil  $\Delta P$  (dotted line corresponds to unlimited  $G_{\text{max}}$  as in Fig. S5). The empirical range was mostly covered (Fig. 6, gray symbols), entirely so at higher  $G_{\text{max}}$ . An increase in the % rhizosphere setting (above 5% default) was able to produce slopes of zero (perfect anisohydry) and below (Fig. S6).

### Responses to soil heterogeneity

Responses to soil heterogeneity were determined by dividing the root zone into  $N$  soil layers of differing  $P_{\text{soil}}$ . A  $P_{\text{soil}}$  profile

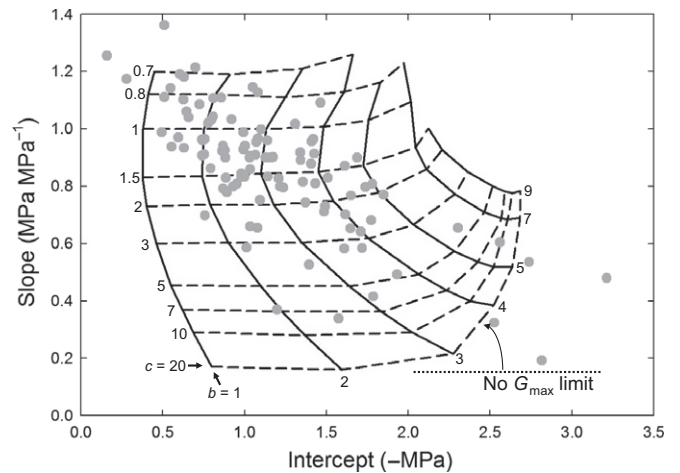


**Fig. 6** Theoretical effect of vulnerability curves on canopy xylem pressure ( $P_{\text{canopy}}$ ) regulation (other settings = default). The slope of the midday vs predawn  $P_{\text{canopy}}$  relationship (linear regression from 0 to 75% loss of plant hydraulic conductance) increases from  $c. 0.2$  (most isohydric) to 1.2 (most anisohydric) as the shape parameter ( $c$ , dashed horizontal curves) of the Weibull function vulnerability curve changes from extreme sigmoidal ( $c=20$ ) to extreme exponential ( $c=0.7$ ). The intercept (the soil–canopy pressure drop for wet soil) increases as the Weibull  $b$  parameter (solid vertical curves) increases up to the point where  $G_{\text{max}}$  limits the pressure drop. Without a  $G_{\text{max}}$  limit, the intercept would continue to increase (dotted line; Supporting Information Fig. S5). Gray symbols are data from Martínez-Vilalta *et al.* (2014).

(Fig. 7, black symbols and line) resulted in a flow profile (Fig. 7, gray symbols and line), which predicted hydraulic redistribution from wet to dry layers when  $E$  was low. For 'predawn' conditions where  $E=0$ , the point on the flow profile where water was neither taken up nor released (Fig. 7, zero flow line) coincided with the predawn xylem pressure on the  $P_{\text{soil}}$  profile (Fig. 7, predawn arrow). This was true regardless of the shape of the  $P_{\text{soil}}$  profile.

The model's steady-state outputs were dependent solely on the predawn xylem pressure, regardless of the underlying heterogeneity of  $P_{\text{soil}}$ . Numerically identical results were obtained whether there were  $N>1$  layers vs  $N=1$ , as long as the predawn xylem pressure was identical (data not shown). This important result simplified model testing because predawn xylem pressure could substitute for usually incomplete measurements of soil moisture and root profiles.

### Influence of vulnerability segmentation

Vulnerability segmentation refers to differences in vulnerability curves along the soil–plant continuum (Tyree *et al.*, 1993). The simulations shown so far (Figs 2–7) assumed no xylem segmentation. But the rhizosphere curve (Eqn 2) is inevitably different from any xylem curve (Eqn 1). The setting for the average % of rhizosphere resistance determines whether flow is more limited by the rhizosphere or the xylem. The default of 5% corresponded to a xylem-limited continuum. This setting assumes that the plant invests sufficiently in root area (and hence rhizosphere  $k_{\text{max}}$ ) to realize the xylem's potential for water extraction. The average rhizosphere resistance had to be increased from 1% to

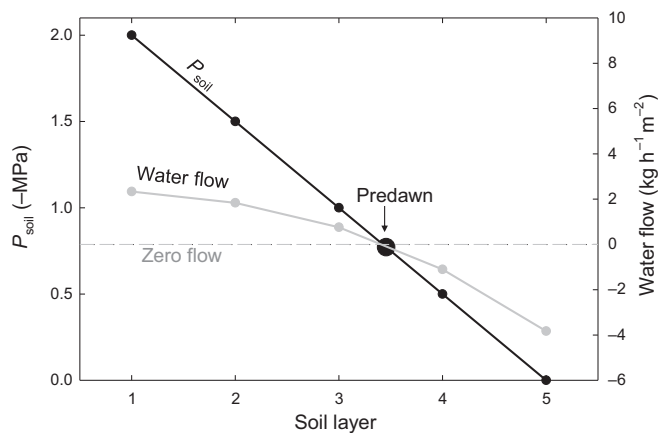


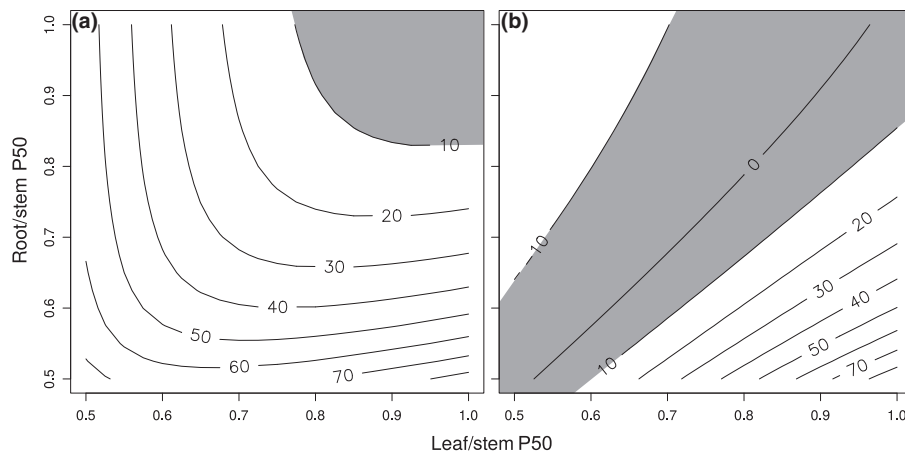
**Fig. 7** Theoretical hydraulic redistribution (gray, flow curve) and predawn xylem pressure (labeled circle) when  $E = 0$ , as driven by heterogeneous soil water potential ( $P_{soil}$ ) across progressively deeper (1, shallowest) soil layers (black line). Negative water flow is water entering the roots in deep, relatively wet soil, and positive flow is water exiting roots into shallow, dry soil. The predicted predawn corresponds with the point in the  $P_{soil}$  profile where water is neither entering nor leaving the root system (dashed, zero flow line).

between 10% (clay, fine-textured extreme) and 20% (sandy loam, coarse-textured extreme) before the reduction in  $E$  (averaged over the  $P_{soil}$  range permitting  $E > 0$ ) exceeded 5% because of an increasing soil limitation.

A single xylem vulnerability curve required only one version of Eqn 1 and eliminated the need to parse continuum  $k_{max}$  into root, stem, and leaf components. However, the typical segmentation is for roots and leaves to be more vulnerable than stems (Sperry *et al.*, 2002b; Hao *et al.*, 2008). If the more available stem vulnerability curve was applied throughout as a substitute for typical segmentation,  $E$  was overpredicted (Fig. 8a). However, as long as root and/or leaf P50 was within  $0.85 \times$  stem P50 (assuming sigmoidal curves that vary  $b$  for constant  $c = 3$  in Eqn 1), the overestimation was  $< 10\%$  (comparing mean  $E$  values across the full  $E > 0$  range; Fig. 8(a), shaded area).

The best no-segmentation substitute curve was the combined stem and leaf vulnerability curve (Fig. 8b). This curve was found by fitting a new Weibull function to the in-series leaf and stem  $k$  computed from Eqn 1. By substituting the combined leaf-stem

**Fig. 8** Theoretical % error in canopy transpiration ( $E$ , labeled contours) when a single vulnerability curve is substituted for true vulnerability segmentation. Segmentation assumed a constant stem curve and P50 (pressure at 50% loss of hydraulic conductance); leaf and root P50 values were reduced to 0.5 of the stem P50 (by reducing  $b$  in Eqn 1). Errors are the % difference between average  $E$  over the full  $P_{soil}$  range permitting  $E > 0$ ; shaded areas  $< 10\%$ . (a) Substitute curve is the stem curve. (b) Substitute curve is the combined stem + leaf curve.



curve, the actual leaf and root P50 could drop below  $0.5 \times$  stem P50 without causing  $> 10\%$  error as long as leaf and root P50 values were within  $c. 30\%$  of each other (Fig. 8b, shaded area). Outside of this zone, error increased, especially if roots were much more vulnerable than leaves. If the root, stem, and leaf curves are all known, a near perfect substitute curve could be solved for by retrofitting the nonsegmented model to its previous segmented output.

### Quantitative model tests

In irreversible cavitation mode, the model tracked the large range in  $G$  and  $P_{canopy}$  associated with wide swings in soil moisture across the nine empirical data sets (Fig. 9; Table 2; individual time series in Figs S7–S11). The model explained 30–93% of the variation in measured  $G$ , and 30–94% of the variation in measured  $P_{canopy}$  (Table 2). Dropping the poor fit to one tropical tree (*Bursera simaruba*; Table 2), the average  $r^2$  values were  $r^2 = 0.76$  (range 0.56–0.93) for  $G$  and  $r^2 = 0.69$  (0.30–0.94) for  $P_{canopy}$ . The absolute error in  $P_{canopy}$  (absolute value of measured vs modeled difference) across all data sets averaged 0.29 MPa. In relative terms, the  $P_{canopy}$  error averaged 15.0% of the mean measured value per data set (range: 11.4–23.3% Table 2; excluding *B. simaruba*). The % error in  $G$  averaged 31.4% (13.2–38.5). The best fits were obtained at  $G_{max}$  averaging 4.1 standard deviations above the observed mean  $G$ , and  $k_{max}$  averaging 2.7 standard deviations above mean  $k$  (Table 2), consistent with  $D$  and cavitation tending to reduce measured values below their maxima. Fitting resulted in a consistently high value for % rhizosphere resistance (67% on average (range 43–86%); Table 2).

The poor fit to *B. simaruba* (and, to a lesser extent, *P. edulis*) was associated with inability to track high-amplitude  $G$  fluctuations in the absence of corresponding shifts in  $P_{soil}$  or  $D$  (Figs S8a,b, S11c,d). These species also exhibited midday xylem pressures that were often less negative than predawn values during dry periods (Wolfe *et al.*, 2016). This cannot be predicted by the model with only one soil layer.

The model fit in reversible cavitation mode was essentially indistinguishable from the irreversible fit (Table S2; Fig. S12). There was no major effect on  $P_{canopy}$  as expected from the model assumption that the soil to canopy pressure drop is unaltered by

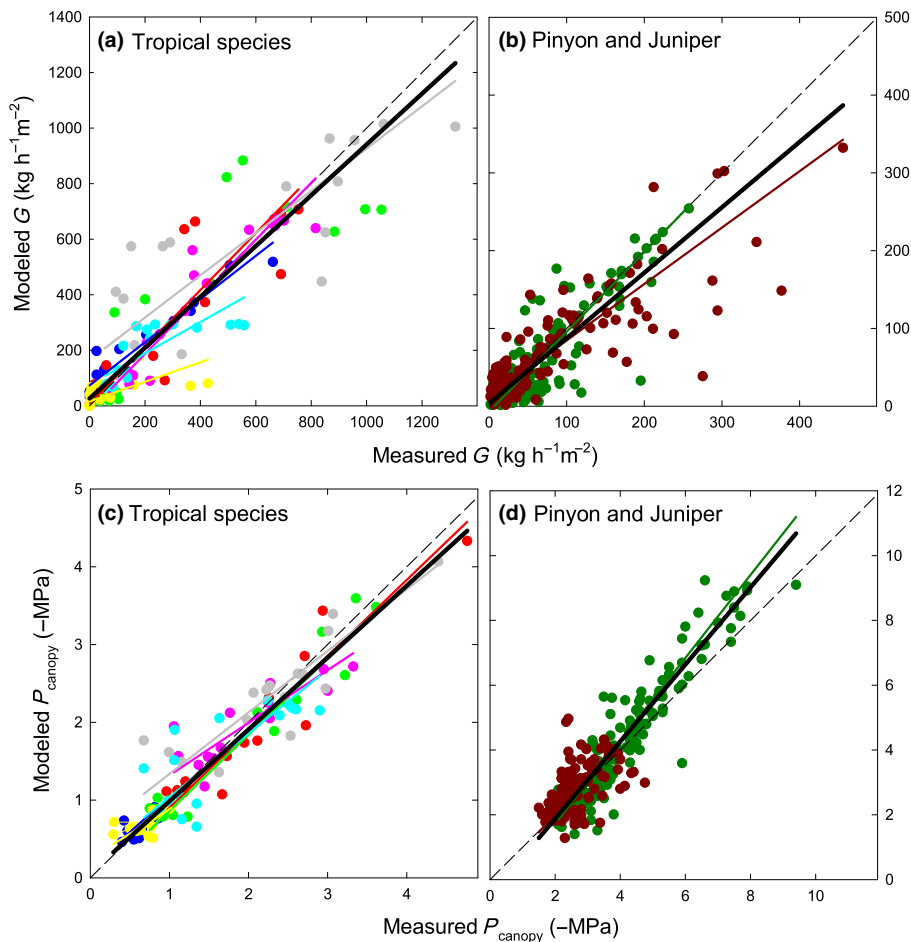


**Fig. 9** Modeled vs measured canopy diffusive conductance ( $G$ ; a, b) and xylem pressure ( $P_{\text{canopy}}$ ; c, d) for the seven tropical (a, c) and two piñon–juniper (b, d) data sets. Reduced major axis regressions are shown for each data set (colored lines) and the entire panel (black line), along with a dashed 1 : 1 line. Light green, *Annona*; cyan, *Astronium*; yellow, *Bursera*; blue, *Cavanillesia*; pink, *Cojoba* transitional dry; gray, *Cojoba* dry; red, *Genipa*; dark green, *Juniperus*; dark red, *Pinus*. The model was set to irreversible cavitation.

previous drought. The fit to  $G$  was also practically the same: the average  $r^2$  per data set was unchanged at 0.76, and the error per data set averaged 31.5% (vs 31.4%, excluding *B. simaruba*; refilling did not improve this fit, nor that of *P. edulis*). The  $G_{\text{max}}$  and  $k_{\text{max}}$  required to achieve the similar fit dropped in at least seven of the nine data sets, by an average of 26% ( $G_{\text{max}}$ ) and 29% ( $k_{\text{max}}$ ), compensating for the refilling setting. There was only minor reduction in the average % rhizosphere setting to an average of 64% from 67%.

## Discussion

The supply–demand theory captured observed trends in stomatal regulation of  $E$  and  $P_{\text{canopy}}$  in response to  $D$  and soil drought while also explaining differences in response sensitivity. With 13 inputs (Table 1), model implementation was relatively simple. The parameters are all traits, most which are measurable. Although vulnerability curves are essential, they are plentiful, and it is arguable that they are required if stomatal responses to drought are ever to be predicted effectively. Any continuum model with water flux that incorporates soil physics (and most do), should be incorporating the analogous physics of xylem.

Importantly, the supply–demand model predicted empirical response functions rather than being based on them. The theoretical  $D$  response was approximated by empirical  $D$  models, but

the theory avoids having to know how empirical coefficients (e.g.  $g_0$ ,  $g$ ,  $m$ ) shift between functional types and with drying soil. The slight decrease in  $E$  at high  $D$  that is seen in some data sets (Monteith, 1995), and which can also cause the slope of  $m$  vs  $G_{\text{ref}}$  to exceed 0.6 (Fig. 3b; Oren *et al.*, 1999), is at variance with the theoretical saturation of  $E$  (Fig. 2). However, even a slight decline in  $P_{\text{soil}}$  can cause  $E$  to decline independently of  $D$  (Fig. 4), suggesting the difficulty of measuring a pure  $D$  response (particularly in the field where high  $D$  often corresponds with drier soil).

The supply–demand theory integrates the  $D$  response with the soil drying response without requiring an empirical soil moisture response function (Fig. 4). Many large-scale models rely on a ‘water stress factor’ (Jarvis, 1976; Stewart, 1988; Powell *et al.*, 2013) that reduces  $G$  at a given  $D$  as needed to obtain closure as soil water content drops (e.g. scaling the empirical  $D$  response equation). The mathematical form of the water stress factor is even less constrained than empirical models of the  $D$  response (Powell *et al.*, 2013), which leads to a poor ability to predict the drought response and how it differs across species.

Empirical response functions for  $P_{\text{canopy}}$  have also been proposed for distinguishing functional types in models. The slope of midday  $P_{\text{canopy}}$  response to predawn xylem pressure (e.g., Fig. 5) can quantify the iso- (slope closer to 0) to anisohydric (slope closer to 1 or above) spectrum (Martínez-Vilalta *et al.*, 2014). Theory predicted nearly the full empirical range of slopes

(0.2–1.4) and  $\Delta P$  intercepts (Fig. 6). For the nonsegmented, xylem-limited model (Fig. 6), exponential vulnerability curves (Weibull  $c \leq 1$ ) produced a slope of 1 ('isohydrodynamic'; Franks *et al.*, 2007) or above ('extreme anisohydry'; Martínez-Vilalta *et al.*, 2014) and sigmoidal curves ( $c \gg 1$ ) produced shallower slopes. In segmented mode, however, the impact of any particular curve shape (rhizosphere, root, stem, leaf) will be damped by the integrated influence of all curves in the network.

The supply–demand model explained most of the variation (up to 94%) in measured  $P_{\text{canopy}}$  and  $G$  in response to wide fluctuations in environmental conditions with an average mean absolute error < 26% (Figs 9, S7–S11; Table 2). The small difference between reversible vs irreversible model fit resulted from adjustment of the fitting parameters ( $G_{\text{max}}$ , continuum  $k_{\text{max}}$ , % rhizosphere resistance) in response to changing the reversibility setting. The data sets lacked conditions for robust estimates of  $G_{\text{max}}$  and  $k_{\text{max}}$  (low  $D$ , high light, prolonged wet soil record), which would allow for a better test of the influence of reversibility. The % rhizosphere resistance is difficult to measure directly (Bristow *et al.*, 1984) and will probably always be a tunable parameter.

The % rhizosphere resistance required to fit the model was much higher (67% on average) than the 10–20% xylem vs soil threshold, suggesting a strong soil limitation. However, it is likely that high soil vulnerability was substituting in part for missing leaf and root vulnerability curves. Leaves and roots are often more sensitive to cavitation than stems, and can greatly influence the model (Fig. 8) in the same general way as an increased soil limitation. Model experiments on our data sets (Notes S1) demonstrated that segmented output (root and leaf P50 half that of the stem) at a 5% rhizosphere setting could be fitted with unsegmented output (stem only) by tuning  $G_{\text{max}}$ ,  $k_{\text{max}}$ , and % rhizosphere. Rhizosphere % increased to an average of 76% and error dropped to an average of 25% (from 144%).  $G_{\text{max}}$  and  $k_{\text{max}}$  changed comparatively little. The % rhizosphere and error values in these simulated fits were typical of our best actual fits (Table 2), indicating that elevated rhizosphere resistance could indeed be compensating for missing segmentation. More rigorous theory testing will require data sets collected for the purpose.

Vulnerability segmentation of xylem is a practical hurdle to implementing the theory. Although stem vulnerability curves are common, root and leaf curves are much less so. If more segmentation data were collected, patterns should emerge that would simplify parameterization. Our sensitivity analysis suggests that if the root/stem and leaf/stem P50 ratios are between 0.85 and 1.0, the root and leaf curves can be ignored (Fig. 8a). Unfortunately, a sampling of the literature produced only *c.* 4% of root vs stem comparisons (24 species, Sperry *et al.*, 2002b) and 12% of leaf vs stem comparisons (17 species, Tyree *et al.*, 1993; Jacobson *et al.*, 2007; Hao *et al.*, 2008; Brodribb & Cochard, 2009; Scoffoni *et al.*, 2011) in this category. Alternatively, if the root/stem and leaf/stem P50 ratios are similar, a combined branch plus leaf curve may be an adequate substitute (Fig. 8b). In the same literature sample, the root/stem P50 ratio ranged from 0.15 to 0.95 and the leaf/stem P50 ratio was in the range 0.36–1.2. Although these ratios were from different species, their similar range is consistent with a similar magnitude in vulnerability segmentation of

roots and leaves. A combined branch plus leaf vulnerability curve can be measured in combination using the dehydration method (Kolb *et al.*, 1996) and may be the best option if just a single curve is used. It was possible to obtain a single xylem curve that accurately represented segmentation, but this required knowing the segmentation, or else solving for a 'hybrid' xylem curve by fitting data. Identifying emergent patterns of vulnerability segmentation would make this single-curve approach feasible.

A broader impact of supply–demand theory is to improve inputs into models of larger-scale processes, thereby improving predictions of responses to water deficits in air and soil. The theoretical  $E$  response in tandem with a layered root system constrains hydrologic models of soil water draw-down and ecosystem water flux (Brooks *et al.*, 2011; Chen *et al.*, 2015). The water-limited  $G$  response can be translated into drought-limited photosynthesis and productivity by existing models (Farquhar & Caemmerer, 1982; Le Roux *et al.*, 2001). The TREES model is an example of how hydraulic constraints on  $G$  can be integrated with stomatal responses to light,  $\text{CO}_2$ , and photosynthetic rate (Mackay *et al.*, 2015). The  $P_{\text{canopy}}$  response limits tissue growth, turgor, and phloem transport (Tyree & Hammel, 1972; Cosgrove, 1997; Sevanto, 2014). The cavitation response contributes to drought memory (Anderegg *et al.*, 2013, 2015). Although all of these responses can contribute to tree mortality, the linkage is best established for the cavitation response. Cavitation-induced losses of 60% or more in tree hydraulic conductance are associated with subsequent mortality (Rice *et al.*, 2004; Hoffmann *et al.*, 2011; Anderegg *et al.*, 2012; Kukowski *et al.*, 2013; McDowell *et al.*, 2013; Urli *et al.*, 2013; Anderegg, 2014). A mortality threshold < 100% suggests death can occur without complete loss of a water supply. Thus, even a stomatal demand function that avoids  $E_{\text{crit}}$  can ultimately be lethal, owing to complications from low gas exchange and extreme  $P_{\text{canopy}}$ .

## Acknowledgements

Funded by National Science Foundation IOS-1450650, IOS-1450679, and the Department of Energy, Survival Mortality and Next Generation Ecosystem Experiment-Tropics. The manuscript benefited from thorough comments by three anonymous reviewers.

## Author contributions

J.S.S. led theory development, wrote the VBA model, designed the research, led the analysis, and wrote the paper. Y.W. participated in theory development, wrote the C model version, and assisted in analysis. B.T.W. collected data on tropical forest species, and assisted in model analysis. D.S.M. and W.R.L.A. assisted in theory development and edited the manuscript. N.G.M. provided data on pinyon pine and juniper, and edited the manuscript. W.T.P. provided data on pinyon pine and juniper.

## References

Allen C, Macalady A, Chenchouni H, Bachelet D, McDowell N, Vennetier M, Kitzberger T, Rigling A, Breshears D, Hogg EH *et al.* 2010. A global

- overview of drought and heat-induced tree mortality reveals emerging climate change risks for forests. *Forest Ecology and Management* 259: 660–684.
- Anderegg WRL. 2014. Spatial and temporal variation in plant hydraulic traits and their relevance for climate change impacts on vegetation. *New Phytologist* 205: 1008–1014.
- Anderegg WRL, Anderegg LDL, Berry JA, Field CB. 2014. Loss of whole-tree hydraulic conductance during severe drought and multi-year forest die-off. *Oecologia* 175: 11–23.
- Anderegg WRL, Berry JA, Smith DD, Sperry JS, Anderegg LDL, Field CB. 2012. The roles of hydraulic and carbon stress in a widespread climate-induced forest die-off. *Proceedings of the National Academy of Sciences, USA* 109: 233–237.
- Anderegg WRL, Placova L, Anderegg LDL, Hacke UG, Berry JA, Field CB. 2013. Drought's legacy: hydraulic deterioration underlies widespread aspen die-off and portends increased future vulnerability. *Global Change Biology* 19: 1188–1196.
- Anderegg WRL, Schwalm C, Biondi F, Camarero JJ, Koch G, Litvak M, Ogle K, Shaw JD, Shevliakova E, Williams AP *et al.* 2015. Pervasive drought legacies in forest ecosystems and their implications for carbon cycle models. *Science* 349: 528–532.
- Ball JT, Woodrow IE, Berry JA. 1987. A model predicting stomatal conductance and its contribution to the control of photosynthesis under different environmental conditions. In: Biggins J, ed. *Progress in photosynthesis research*, vol 4. Leiden, the Netherlands: Martinus Nijhoff, 221–224.
- Bristow KL, Campbell GS, Calissendorff C. 1984. The effects of texture on the resistance to water movement within the rhizosphere. *Soil Science Society of America Journal* 48: 266–270.
- Brodribb TJ, Cochard H. 2009. Hydraulic failure defines the recovery and point of death in water-stressed conifers. *Plant Physiology* 149: 575–584.
- Brooks PD, Troch PA, Durcik M, Gallo E, Schlegel M. 2011. Quantifying regional-scale ecosystem responses to changes in precipitation: not all rain is created equal. *Water Resources Research* 47: W00J08.
- Brown HR. 2013. The theory of the rise of sap in trees: some historical and conceptual remarks. *Physics in Perspective* 15: 320–358.
- Buckley TN, Mott KA. 2013. Modelling stomatal conductance in response to environmental factors. *Plant, Cell & Environment* 36: 1691–1699.
- Chen L, Wang L, Ma Y, Liu P. 2015. Overview of ecohydrological models and systems at the watershed scale. *IEEE Systems Journal* 9: 1091–1099.
- Comstock JP, Sperry JS. 2000. Theoretical considerations of optimal conduit length for water transport in vascular plants. *New Phytologist* 148: 195–218.
- Cosgrove DJ. 1997. Relaxation in a high-stress environment: the molecular bases of extensible cell walls and cell enlargement. *Plant Cell* 9: 1031–1041.
- Cowan IR. 1977. Stomatal behaviour and the environment. *Advances in Botanical Research* 4: 117–228.
- Dai A. 2011. Drought under global warming: a review. *WIREs Climate Change* 2: 45–65.
- Farquhar GD, Caemmerer SV. 1982. Modelling of photosynthetic response to environmental conditions. In: Lange OL, Nobel PS, Osmond CB, Ziegler H, eds. *Physiological plant ecology II: water relations and carbon assimilation*. Berlin, Germany: Springer-Verlag, 549–587.
- Field CB, Holbrook NM. 1989. Catastrophic xylem failure: life at the brink. *Trends in Ecology and Evolution* 4: 124–126.
- Franks PJ. 2013. Passive and active stomatal control: either or both? *New Phytologist* 198: 325–327.
- Franks PJ, Drake PL, Froend RH. 2007. Anisohydric but isohydrodynamic: seasonally constant plant water potential gradient explained by a stomatal control mechanism incorporating variable plant hydraulic conductance. *Plant, Cell & Environment* 30: 19–30.
- van Genuchten MT. 1980. A closed form equation for predicting the hydraulic conductivity of unsaturated soils. *Soil Science Society of American Journal* 44: 892–898.
- Hacke UG, Sperry JS, Ewers BE, Ellsworth DS, Schäfer KVR, Oren R. 2000. Influence of soil porosity on water use in *Pinus taeda*. *Oecologia* 124: 495–505.
- Hao GY, Hoffmann W, Scholz FG, Bucci SJ, Meinzer FC, Franco AC. 2008. Stem and leaf hydraulics of congeneric tree species from adjacent tropical savanna and forest ecosystems. *Oecologia* 155: 405–415.
- Hoffmann WA, Marchin RM, Abit P, Lau OL. 2011. Hydraulic failure and tree dieback are associated with high wood density in a temperate forest under extreme drought. *Global Change Biology* 17: 2731–2742.
- Jackson RB, Canadell J, Ehleringer JR, Mooney HA, Sala OE, Schulze ED. 1996. A global analysis of root distributions for terrestrial biomes. *Oecologia* 108: 389–411.
- Jacobson AL, Pratt RB, Ewers FW, Davis SD. 2007. Cavitation resistance among 26 chaparral species of southern California. *Ecological Monographs* 77: 99–115.
- Jarvis PG. 1976. The interpretation of the variations in leaf water potential and stomatal conductance found in canopies in the field. *Philosophical Transactions of the Royal Society of London Series B, Biological Sciences* 273: 593–610.
- Jones HG, Sutherland R. 1991. Stomatal control of xylem embolism. *Plant, Cell & Environment* 14: 607–612.
- Kolb KJ, Sperry JS, Lamont BB. 1996. A method for measuring xylem hydraulic conductance and embolism in entire root and shoot systems. *Journal of Experimental Botany* 47: 1805–1810.
- Kukowski K, Schwinning S, Schwartz B. 2013. Hydraulic responses to extreme drought conditions in three co-dominant tree species in shallow soil over bedrock. *Oecologia* 171: 819–830.
- Le Roux X, Lacoïnte A, Escobar-Gutiérrez A, Le Dizès S. 2001. Carbon-based models of individual tree growth: a critical appraisal. *Annals of Forest Science* 58: 469–506.
- Leij FJ, Alves WJ, Van Genuchten MT, Williams JR. 1996. *Unsaturated soil hydraulic database UNSODA 1.0 User's Manual*, v. EPA Report 600/R-96/095. Ada, OK, USA: USEPA.
- Leuning R. 1995. A critical appraisal of a coupled stomatal-photosynthesis model for C<sub>3</sub> plants. *Plant, Cell & Environment* 18: 339–357.
- Li S, Assmann SM, Albert R. 2006. Predicting essential components of signal transduction networks: a dynamic model of guard cell abscisic acid signaling. *PLoS Biology* 4: e312.
- Lloyd J. 1991. Modeling stomatal responses to environment in *Macadamia integrifolia*. *Australian Journal of Plant Physiology* 18: 649–660.
- Mackay DS, Roberts DE, Ewers BE, Sperry JS, McDowell N, Pockman W. 2015. Interdependence of chronic hydraulic dysfunction and canopy processes can improve integrated models of tree response to drought. *Water Resources Research* 51: 6156–6176.
- Martínez-Vilalta J, Poyatos R, Aguadé D, Retana J, Mencuccini M. 2014. A new look at water transport regulation in plants. *New Phytologist* 204: 105–115.
- McDowell NG, Fisher RA, Xu C, Domec JC, Hölttä T, Mackay DS, Sperry JS, Boutz A, Diskman L, Geheres N *et al.* 2013. Evaluating theories of drought-induced vegetation mortality using a multimodel-experimental framework. *New Phytologist* 200: 304–321.
- Medlyn BE, Duursma RA, Eamus D, Ellsworth DS, Prentice IC, Barton CVM, Crous KY, de Angelis P, Freeman M, Wingate L. 2011. Reconciling the optimal and empirical approaches to modelling stomatal conductance. *Global Change Biology* 17: 2134–2144.
- Milburn JA. 1973. Cavitation in *Ricinus* by acoustic detection: induction in excised leaves by various factors. *Planta* 110: 253–265.
- Milburn JA. 1979. *Water flow in plants*. London, UK: Longman.
- Monteith JL. 1995. A reinterpretation of stomatal response to humidity. *Plant, Cell & Environment* 18: 357–364.
- Nelder JA, Mead R. 1965. A simplex method for function minimization. *Computer Journal* 7: 308–313.
- Oren R, Sperry JS, Katul GG, Pataki DE, Ewers BE, Phillips N, Schafer KVR. 1999. Survey and synthesis of intra- and interspecific variation in stomatal sensitivity to vapour pressure deficit. *Plant, Cell & Environment* 22: 1515–1526.
- Pickard WF. 1981. The ascent of sap in plants. *Progress in Biophysics and Molecular Biology* 37: 181–229.
- Pieruschka R, Huber G, Berry JA. 2010. Control of transpiration by radiation. *Proceedings of the National Academy of Sciences, USA* 107: 13372–13377.
- Powell TL, Galbraith DR, Christoffersen BO, Harper A, Imbuzeiro HMA, Rowland L, Almeida S, Brando PM, da Costa ACL, Costa MH *et al.* 2013. Confronting model predictions of carbon fluxes with measurements of Amazon forests subjected to experimental drought. *New Phytologist* 200: 350–365.

- Press WH, Flannery BP, Teukolsky SA, Vetterling WT. 1989. *Numerical recipes in Pascal*. Cambridge, UK: Cambridge University Press.
- Rice KJ, Matzner SL, Byer W, Brown JR. 2004. Patterns of tree dieback in Queensland, Australia: the importance of drought stress and the role of resistance to cavitation. *Oecologia* 139: 190–198.
- Saliendra NZ, Sperry JS, Comstock JP. 1995. Influence of leaf water status on stomatal response to humidity, hydraulic conductance, and soil drought in *Betula occidentalis*. *Planta* 196: 357–366.
- Scoffoni C, Rawls M, McKown A, Cochard H, Sack L. 2011. Decline of leaf hydraulic conductance with dehydration: relationship to leaf size and venation architecture. *Plant Physiology* 156: 832–843.
- Sevanto S. 2014. Phloem transport and drought. *Journal of Experimental Botany* 65: 1751–1759.
- Sparks JP, Black RA. 1999. Regulation of water loss in populations of *Populus trichocarpa*: the role of stomatal control in preventing xylem cavitation. *Tree Physiology* 19: 453–459.
- Sperry JS, Adler FR, Campbell GS, Comstock JP. 1998. Limitation of plant water use by rhizosphere and xylem conductance: results from a model. *Plant, Cell & Environment* 21: 347–359.
- Sperry JS, Hacke UG, Oren R, Comstock JP. 2002a. Water deficits and hydraulic limits to leaf water supply. *Plant, Cell & Environment* 25: 251–263.
- Sperry JS, Love DM. 2015. What plant hydraulics can tell us about plant responses to climate-change droughts. *New Phytologist* 207: 14–27.
- Sperry JS, Stiller V, Hacke UG. 2002b. Soil water uptake and water transport through root systems. In: Waisel Y, Eshel A, Kafkafi U, eds. *Plant roots: the hidden half*. New York, NY, USA: Marcel Dekker, 663–681.
- Stewart JB. 1988. Modelling surface conductance of pine forest. *Agricultural and Forest Meteorology* 43: 16–35.
- Tardieu F, Davies WJ. 1993. Root-shoot communication and whole-plant regulation of water flux. In: Davies WJ, ed. *Water deficits: plant responses from cell to community*. Lancaster, UK: BIOS Scientific Publishers, 147–162.
- Tombesi S, Nardini A, Frioni T, Soccolini M, Zadra C, Farinelli D, Poni S, Palliotti A. 2015. Stomatal closure is induced by hydraulic signals and maintained by ABA in drought-stressed grapevine. *Scientific Reports* 5: 12449.
- Tyree MT, Cochard H, Cruziat P, Sinclair B, Ameglio T. 1993. Drought-induced leaf shedding in walnut – evidence for vulnerability segmentation. *Plant, Cell & Environment* 16: 879–882.
- Tyree MT, Hammel HT. 1972. The measurement of the turgor pressure and the water relations of plants by the pressure-bomb technique. *Journal of Experimental Botany* 23: 267–282.
- Tyree MT, Sperry JS. 1988. Do woody plants operate near the point of catastrophic xylem dysfunction caused by dynamic water stress? Answers from a model. *Plant Physiology* 88: 574–580.
- Urli M, Porte AJ, Cochard H, Guengant Y, Burlett R, Delson S. 2013. Xylem embolism threshold for catastrophic hydraulic failure in angiosperm trees. *Tree Physiology* 33: 672–688.
- Williams M, Rastetter EB, Fernandes DN, Goulden ML, Wofsy SC, Shaver GR, Melillo JM, Munger JW, Fan SM, Nadelhoffer KJ. 1996. Modelling the soil-atmosphere continuum in a Quercus-Acer stand at Harvard Forest: the regulation of stomatal conductance by light, nitrogen and soil/plant hydraulic properties. *Plant, Cell & Environment* 19: 911–927.
- Wolfe BT, Sperry JS, Kursar TA. 2016. Does leaf shedding protect stems from cavitation during seasonal droughts? A test of the hydraulic fuse hypothesis. *New Phytologist* (In Press). doi: 10.1111/nph.14087.

## Supporting Information

Additional Supporting Information may be found online in the Supporting Information tab for this article:

**Fig. S1** Vulnerability curves for modeled species.

**Fig. S2** Vulnerability curves for sensitivity analysis.

**Fig. S3** Sensitivity of canopy diffusive conductance ( $G$ ) to vapor pressure deficit ( $D$ ).

**Fig. S4** Sensitivity of canopy diffusive conductance ( $G$ ) to soil water potential ( $P_{\text{soil}}$ ).

**Fig. S5** Fig. 6 from the text, but with unlimited maximum canopy diffusive conductance ( $G_{\text{max}}$ ).

**Fig. S6** Effect of the % rhizosphere setting on Fig. S5.

**Figs S7–S11** Time sequence of modeled vs measured  $G$  and  $P_{\text{canopy}}$  for each modeled species.

**Fig. S12** Model vs measured  $G$  and  $P_{\text{canopy}}$  for reversible cavitation mode.

**Table S1** Data set parameters

**Table S2** Model fit statistics for reversible cavitation mode

**Methods S1** Model fitting.

**Notes S1** Model experiments on % rhizosphere compensation.

Please note: Wiley Blackwell are not responsible for the content or functionality of any supporting information supplied by the authors. Any queries (other than missing material) should be directed to the *New Phytologist* Central Office.